Influence of Polarization on Structural, Thermodynamic, and Dynamic Properties of Ionic Liquids Obtained from Molecular Dynamics Simulations

Dmitry Bedrov,[†,‡] Oleg Borodin,[†,‡] Zhe Li,[†] and Grant D. Smith[†]

Department of Materials Science & Engineering, University of Utah, 122 South Central Campus Drive, Rm 304, Salt Lake City, Utah 84112, and Wasatch Molecular Inc., 2141 Saint Mary's Drive, Salt Lake City, Utah 84108

Received: December 9, 2009; Revised Manuscript Received: February 11, 2010

Utilizing the transferable, quantum-chemistry-based, Atomistic Polarizable Potential for Liquids, Electrolytes, & Polymers (APPLE&P) force field, we have systematically investigated the influence of polarization effects on the accuracy of properties predicted from molecular dynamics simulations of various room temperature ionic liquids (ILs). Simulations of ILs in which the atom-based polarizability was set to zero for all atoms (nonpolarizable APPLE&P potential) resulted in changes in thermodynamic and dynamic properties from those predicted by the polarizable APPLE&P potential that are qualitatively different from changes observed for nonionic liquids. Investigation of structural and dynamical correlations using both the polarizable and nonpolarizable versions of APPLE&P allowed us to obtain a mechanistic understanding of the influence of polarization on dynamics in the ILs investigated. Additionally, the Force Matching (FM) approach was employed to systematically obtain nonpolarizable two-body force fields for several ILs that reproduce as accurately as possible intermolecular forces predicted by the polarizable model. Unlike water, for which the FM approach was found to yield an accurate representation of the liquid phase structure predicted by a polarizable model, the FM approach does not result in a two-body potential that accurately reproduces either structure or dynamics predicted by the polarizable IL model.

I. Introduction

Over the past decade, room temperature ionic liquids (ILs) have been widely investigated for a variety of applications, including biphasic systems for separation, solvents for synthetic and catalytic applications,[1] lubricants[2,3] lithium batteries,[4−7] actuators,[8,9] sensors,[10] reaction media[11] replacement of conventional solvents,[12] active pharmaceutical ingredients,[11] and hypergolic propellants.[13] Negligible vapor pressure, good thermal and electrochemical stability, good dissolution with many organic and inorganic compounds, low flammability, and a wide variety of possible anions and cations are a few examples of the characteristics that make ILs exciting alternative materials for many applications. Importantly, IL properties can be tailored for specific chemical (separation, catalysis, reactions, propellants, explosives) or electrochemical (battery, actuators, supercapacitors) applications by tuning the combination of cations and anions to achieve the desired thermodynamic, solvating, and transport properties. However, screening and testing a large number of possible cation/anion combinations presents an enormous challenge for product design because synthesis and characterization of a large number of ILs is expensive. Consequently, molecular dynamics (MD) simulations are emerging as a good complementary (to empirical correlations and experiments) option for prediction of various properties of ILs. Indeed, most structural, thermodynamic, and transport properties of ILs are in principle accessible from MD simulations. Realization of the potential advantages of MD simulations in predicting properties and obtaining fundamental understanding of ILs has sparked tremendous interest in this field, leading to numerous MD simulation studies of ILs with imidazolium,[14−33] pyridinium,[34] pyrrolidinium,[35−37] triazolium,[38,39] tetraalkylphosphonium,[40] and tetraalkylammonium[41−43] cations and a variety of anions.

Although reported MD simulation studies have provided valuable insight into molecular level correlations in ILs, they also have demonstrated that accurate prediction of thermodynamic and transport properties for this class of materials is challenging. Central to accurate prediction of any property from MD simulation is the quality of the force field employed. The predicted thermodynamic and transport properties of ILs from MD simulations are often inconsistent with or in much poorer agreement with experiments than has been typically observed for nonionic liquids. This is particularly true for prediction of transport properties (viscosity, self-diffusion coefficients, and ionic conductivity), for which deviations by almost an order of magnitude from experimental data are typical in MD studies of ILs. For example, the self-diffusion coefficients obtained from simulations using the force field of Padua et al. were a factor of 5 smaller than experimental values for [1-ethyl-3-methylimidazolium][bis(trifluoromethylsulfonyl)imide] (or [emim][Ntf_2])[29] and significantly slower than in experiment for [1,3-dimethylimidizolium][chloride] (or [mmim][Cl]) and [1-butyl,3-methylimidazolium][hexafluorophosphate] (or [bmim][PF_6]).[28] Similarly, a sluggish ion transport has been found in simulations by Picálek et al.[31] of [emim][PF_6], [bmim][PF_6] and [bmim][BF_4] utilizing five different force fields. Maginn's simulations of alkylpyridinium-based ionic liquids predicted apparent self-diffusivities that are roughly 10 times lower than experimental values.[34] Recent simulations of 13 different ILs by Tsuzuki et al.[44] using modified OPLS force field predicted self-diffusion coefficients with deviations from

* Corresponding author. E-mail: bedrov@tacitus.mse.utah.edu.
† University of Utah.
‡ Wasatch Molecular Inc.

10.1021/jp911670f
Published on Web 03/25/2010

experiments ranging from a factor of almost 10 up to as much as a factor of 40.

The majority of MD simulations of ILs reported so far, including the examples mentioned above, have been conducted using atomistic nonpolarizable force fields that are typically tuned to reproduce experimental density and sometimes heat of vaporization. For nonionic liquids, such tuning is usually sufficient to allow reasonable prediction of transport properties, as well. Yet, as illustrated by the mentioned above examples, this approach does not work very well in ILs and is further complicated by the paucity of available experimental data on heats of vaporization for ILs. In some studies, an improved description of dynamical properties was obtained by reducing the ion charges to $0.9e$ or $0.8e$ (e = electron charge).[28,45,46] Moreover, most of the nonpolarizable force fields reported in the literature are specific for the ion pair they were developed for, and therefore, even when there are instances of force fields that accurately reproduce transport and thermodynamic properties for the IL of interest (e.g., the force field of Loddermann, Paschek and Ludwig[29] for [alkylimidazolium][Ntf_2]), the transferability of such a force field to other cations and anions is questionable.

Recently, we developed an Atomistic Polarizable Potential for Liquids, Electrolytes, & Polymers (APPLE&P) and demonstrated that MD simulations using this force field provide an accurate description of thermophysical and transport properties for a large number of ILs.[47] Moreover, the developed APPLE&P database uses the same repulsion−dispersion nonbonded parameters for the same type atoms, in most cases independently of their chemical environment, indicating a high degree of transferability of this force field. Although details of the APPLE&P force field parametrization and validation can be found in ref 47, the unprecedented accuracy and transferability of this force field raise a fundamental question: What role does the inclusion of polarizability play in the success of the APPLE&P force field in predicting the dynamics accurately? And if many-body polarization interactions are essential, can they be replaced by effective two-body interactions and provide similar quality predictions at significantly lower computational expense?

The latter has been already investigated for liquid water by Iuchi et al.[48] In that work, a two-body force field has been obtained from MD simulations with a polarizable water model using the Force Matching approach[49] (described below). Subsequent simulations using the parametrized effective two-body force field predicted basically identical structure and very good agreement of thermodynamic properties with those obtained from simulations using the polarizable water model, whereas the self-diffusion coefficient obtained from simulations using the developed two-body model was 42% larger than that obtained from simulations with the original polarizable model. Taking into account that MD simulations using polarizable force fields are about a factor of 4 more computationally expensive than those using the same potential form without polarization and that many ILs require very long simulation trajectories because of their high viscosity, it would be extremely useful if accurate two-body approximation of many-body interactions could be developed for ILs.

There have been several works that investigated the influence of polarization effects on properties of ILs predicted from MD simulations. Madden and co-workers have simulated several simple molten salts using both polarizable and nonpolarizable models.[50,51] In their investigation of KI/vacuum interfaces,[50] these authors found that inclusion of polarization widens the interfacial region and therefore results in ∼20% lower (compared to simulations with nonpolarizable force field) values of the surface tension. In another study of LiCl and KCl liquids,[51] it was found that inclusion of polarization did not influence the structure of the molten salts but increased the self-diffusion coefficients of all ions by about 10−20% as compared to those obtained from simulations using the same force field with atom-based polarizabilities set to zero. The influence of polarization on structural, thermodynamic, and dynamical properties was already investigated for [emim][NO_3][52,53] and [emim][BF_4].[54] These studies found a significant difference in anion−anion pair distribution functions as well as transport properties obtained from simulations using the polarizable force field and those obtained using the same force field with atom-based polarizabilities set to zero (nonpolarizable force field). The self-diffusion coefficients for both ions at 400 K were found to be a factor of 2−3 larger and viscosity ∼30% lower in simulations with the polarizable model as compared to those from simulations with the nonpolarizable force field.[47,52] The surface tension obtained for the [emim][NO_3]/vacuum interface from simulations that included polarization was more consistent with experimental data and was ∼30% lower than predictions from simulations using a nonpolarizable force field. Hansen and McDonald suggested that inclusion of polarization effects provides additional screening mechanisms that do not require movement of ion cores to provide local charge neutrality.[55] These additional mechanisms cause the cage effect to be smaller for polarizable ions, which should lead to increased damping of oscillations in the velocity autocorrelation function and increased self-diffusion coefficients.

In this manuscript, we systematically investigate the influence of many-body polarization on several important properties of a series of ILs, as predicted from MD simulations. First we investigate the influence of polarization on representative structural, thermodynamic, and dynamic properties of selected ILs by comparing results from MD simulations using the polarizable APPLE&P force field and a nonpolarizable version of the APPLE&P force field in which polarization interactions were simply turned off (i.e., atom-based dipole polarizabilities were set to zero). The influence of polarization on the properties of these ILs is compared with that obtained from simulations of nonionic liquids for which a similar procedure of turning off polarization has been used. We then attempt to systematically develop an effective nonpolarizable force field for selected ILs using the Force Matching approach and discuss the feasibility of replacing many-body polarization interactions with effective two-body interactions.

II. Simulation Details

Systems Studied. For our study, we have selected common yet structurally quite different cations and anions whose molecular structure and simplified notation are shown in Figure 1. Several ILs consisting of these cation/anion combinations have been investigated at atmospheric pressure and two temperatures, 298 and 393 K. The investigated ILs are listed in Table 1, together with available experimental data for density and transport properties.[56−62] As can be seen from Table 1, the viscosity (η) of the select ILs at 298 K ranges from 16 mPa·s for [emim][$N(CN)_2$] up to as much as 99 mPa·s for [N_{1114}][Ntf_2]. Here, we focused on relatively low viscosity ILs to reduce computational costs. We also note that low viscosity is highly desirable for numerous applications from batteries and supercapacitors to hypergolic fuels. Taking into account significant difference in chemical structure and physical properties of the

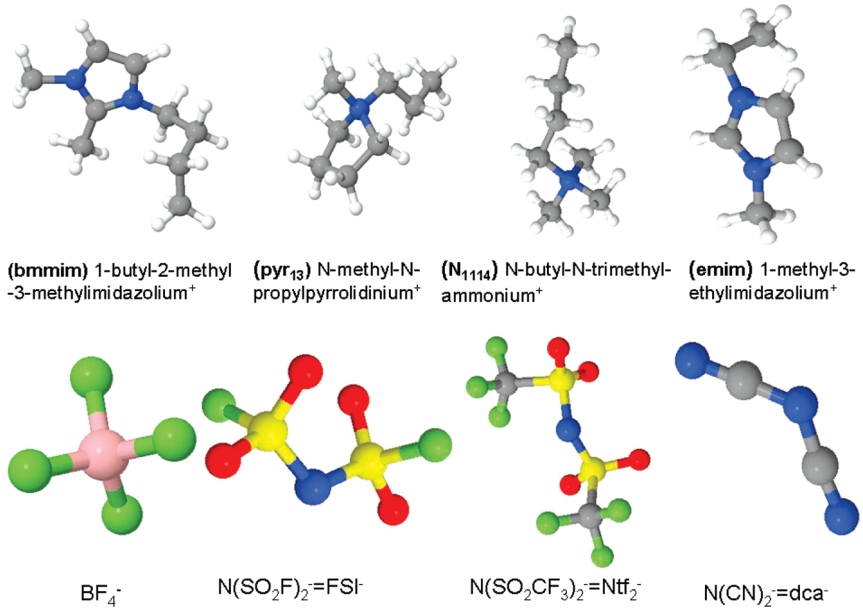

Figure 1. Molecular structure and notation for cations and anions used in our simulations.

TABLE 1: List of Ionic Liquids Selected for This Study Together with Available in the Literature Experimental Data on Density (ρ), Viscosity (η), Self-Diffusion Coefficient (D), and Ionic Conductivity (λ) at 298 K

			D (10^{-10} m^2/s)		
IL	ρ kg/m^3	η mPa·s	cation	anion	λ mS/cm
[emim][BF_4]	1280[56]	38.0[57]	0.497[56]	0.416[56]	13.6−15.7[56]
[emim][FSI]		15.5[58]			15.4[58]
[emim][$N(CN)_2$]	1080[59]	16.1[59]			28.4[59]
[bmmim][Ntf_2]	1420[60]		0.198[60]	0.152[60]	1.6[60]
[N_{1114}][Ntf_2]	1393[59]	99.0[59]	0.131[61]	0.117[61]	2.05[61]
[pyr_{13}][FSI]		39−40[58,62]			6.4,[58] 8.2[62]

selected ILs, we believe that trends and phenomena investigated in this work will be generically applicable to a wide range of ILs.

To determine whether the inclusion of many-body polarization effects is particularly important for ILs, we also investigated several polar but nonionic compounds, such as water, dimethyl ketone (DMK), and ethylene carbonate (EC). All these compounds have relatively large dielectric constants and are considered highly polar fluids. In these liquids, intermolecular electrostatic interactions are strong, and hence, there is a large chance that polarization effects can play a significant role in determining their properties. On the other hand, it is known that in nonpolar liquids (e.g. alkanes), electrostatic interactions do not play an important role in determining properties, and hence, we can hardly expect that polarization interactions will be of any significance in such systems. Therefore, we did not include any nonpolar liquids in our study.

Polarizable Force Field. For all materials investigated (except for water), the APPLE&P force field was used for simulations with many-body polarization effects. Details on the APPLE&P functional forms and parametrization procedure can be found in ref 47. Here, we only briefly highlight the conceptual differences of this force field with other nonpolarizable force fields. As for most atomistic force fields, the APPLE&P force field includes terms describing valence interactions (bonds and bends vibrations, dihedral potential, and out-of-plane deformation) and nonbonded interactions (all intermolecular and intramolecular for atoms separated by three bonds or more). The nonbonded interactions include van der Waals interactions (expressed by Buckingham exponential-6 potential) and electrostatic interactions. The latter, in addition to typical interactions due to fixed partial atomic charges, also include interactions between and with induced point dipoles centered on each atom. The functional form for nonbonded interactions is defined as

$$U^{NB}(\mathbf{r}) = \sum_{i>j}\left(A_{\alpha\beta}\exp(-B_{\alpha\beta}r_{ij}) - C_{\alpha\beta}r_{ij}^{-6} + D\left(\frac{12}{B_{\alpha\beta}r_{ij}}\right)^{12}\right) + \sum_{i>j}\left(\frac{q_iq_j}{4\pi\varepsilon_0 r_{ij}}\right) - 0.5\sum_i \vec{\mu}_i\vec{E}_i^0 \quad (1)$$

where $\vec{\mu}_i = \alpha_i\vec{E}_i^{tot}$ is an induced dipole at force center i, α_i is the isotropic atomic polarizability, $\vec{E}_i^{tot}$ is the total electrostatic field at the atomic site i due to permanent charges q_j and induced dipoles $\vec{\mu}_j$, ε_0 is the dielectric permittivity of vacuum, $\vec{E}_i^0$ is the electric field due to fixed charges only, $A_{\alpha\beta}$ and $B_{\alpha\beta}$ are the repulsion parameters, and $C_{\alpha\beta}$ is the dispersion parameter for interaction between atoms i and j with atom types α and β. The term $D(12/B_{\alpha\beta}r_{ij})^{12}$, with $D = 5 \times 10^{-5}$ kcal/mol for all pair interactions, is essentially zero at typical nonbonded atomic separations but becomes the dominant term at $r_{ij} < 1$ Å, ensuring that that nonbonded interactions are repulsive at distances much smaller than the size of an atom. Intramolecular nonbonded interactions are included for atoms separated by three or more covalent bonds. The Thole screening[63] ($a_T = 0.2$) that smears induced dipoles to prevent the so-called "polarization catastrophe" from occurring. The interaction between an induced dipole and a partial charge separated by three bonds was scaled by 0.8. Total molecular polarizability of ions (defined as a sum of atomic polarizabilities) is given in the Supporting Information.

The polarizable RPOL model of Dang has been used in our simulations of water.[64] This water model has been extensively validated against experimental structural, thermodynamic, and dynamic properties of bulk water and aqueous solutions.[64,65] Below, we will refer to all polarizable models as "POL".

Nonpolarizable Models. In this work, we used several nonpolarizable models. In all these models, all valence and van der Waals interactions were kept the same as in a polarizable force field; only the description of electrostatic interactions was

approximated differently using pairwise interactions. In the first model, the partial atomic charges were kept the same as in the POL force field while atomic polarizabilities were set to zero ($\alpha_i = 0$). In this case, no induced dipoles are created on the atoms, and therefore, electrostatic interactions are reduced only to interactions between fixed partial atomic charges. We will refer to this force field as "NP".

For three systems ([emim][BF_4], [emim][FSI], and [pyr_{13}][FSI]), we also developed nonpolarizable models in which all or a fraction of the electrostatic interactions have been fitted using the Force Matching (FM) methodology. The details of the fitting using the FM methodology are described in the next subsection; here, we introduce only the essences of the obtained models. As in the NP model introduced above, the parameters describing valence and van der Waals interactions were kept the same as in the POL force field, while electrostatic interactions were described by short-range (cutoff 11.0 Å) pairwise interactions represented by numerical functions (each type of the pairwise interaction was described by its own function). In the first model of this type, the numerical functions effectively represented interactions due to induced dipoles (dipole−dipole and dipole−charge), and the charge−charge interactions were described using the same partial atomic charges, including long-range interactions treated by Ewald summation (see below), as in the POL force field. We refer to this model as "NP-FMp". In the second model, all electrostatic interactions were approximated by short-range numerical functions obtained using the FM approach. We refer to this model as "NP-FMe". Since we have not put any constraints on the functional form of those effective two-body interactions approximating electrostatic interactions in the NP-FM models, each type of possible pairwise interaction had its own numerical function. Taking into account that each atom type can have several charge types, depending on the atom chemical environment, the number of different pairwise interactions ranged from 78 to 136, depending on the system, all of which were fitted simultaneously using the FM approach. A list of atom/charge types for systems used in FM fitting are given in the Supporting Information together with the total number of pairwise interactions fitted for each system.

We would like to emphasize that the primary purposes of the simulations using nonpolarizable models discussed above are to facilitate understanding of the influence of polarization interactions on the thermodynamic, structural, and dynamic properties of fluids and correlations between them and to determine if effective two-body potentials can be developed using the FM approach that accurately represent the structure, thermodynamics, and dynamics of the simulated materials yielded by polarizable potentials. It is not the purpose of these studies to develop new nonpolarizable potentials that accurately describe experimentally determined properties for the simulated materials. None of these models has been empirically adjusted to match any experimental data and, hence, in principle cannot be expected to perform as well as some other nonpolarizable models reported in the literature where systematic empirical adjustment of parameters is made to allow better agreement with experimental data. Simulations using the NP model introduced above provide a direct probe of the importance of polarization interactions in the POL model for various properties of the system of interest. As we will show below, in many cases, the NP model provides an inadequate description of the material, indicating that polarization interactions are playing a crucial role in defining the material properties. Therefore, if one develops a nonpolarizable model for simulation of such material, missing polarization interactions have to be effectively approximated through modification of available parameters in the model. Typically, this is done through redistribution of partial atomic charges (i.e., changes of molecular dipole and/or quadrupole moments) or adjustment of parameters for van der Waals interactions. Such an approach certainly can improve agreement between simulation predictions and experimental data for thermophysical properties; however, it relies on different physics (i.e., interactions) to achieve the desired agreement and may result in a poor description of other properties of the material. In parametrization of our NP-FM models, we attempt to overcome this drawback by trying to reproduce polarization interactions directly using effective two-body interactions while keeping all other interactions (due to fixed charges and van der Waals) intact.

Force Matching Protocol. The FM methodology is extensively discussed in a number of papers by Izvekov et al.[48,49,66] Here, we only briefly describe the main concepts and specifics of the fitting procedure applied in this work. To obtain two-body interactions that effectively approximate the many-body interactions due to polarization, we first conduct MD simulations of the system at conditions of interest using the POL force field. For this purpose, we have chosen [emim][BF_4] [emim][FSI] and [pyr_{13}][FSI] at 393 K and atmospheric pressure. During these simulations, the coordinates and the forces due to those interactions that one wishes to approximate using the FM method are recorded for each atom every 50 fs. Since our objective is to approximate either the electrostatic or part of the electrostatic interactions, we recorded only corresponding forces from those interactions (F^{POL}). The forces due to an induced dipole−induced dipole and charge-induced dipole (for the NP-FMp model) or due to all electrostatic interactions (for the NP-FMe model) were recorded. Then every 500 fs (i.e., cumulative of 10 snapshots of statistics), a least-squares minimization of an objective function,

$$\chi^2 = \frac{1}{3NL}\sum_{l=1,L}\sum_{i=1,N}\sum_{j=x,y,z}\left|F_{ilj}^{POL} - F_{ilj}^{NP}\left(f_{k=1,K}^{m=1,M}\right)\right|^2 \quad (2)$$

is conducted. In eq 2 N is a number of atoms in the system, L is a number of snapshots used for statistics, F^{POL} is an x, y, or z component of the force acting on atom i in configuration l obtained using the POL force field, and F^{NP} is a corresponding component of the force on the same atom in the same configuration using the desired nonpolarizable model. The latter depends on $k = 1, K$ number of parameters representing each type $m = 1, M$ of pairwise interactions. Here, each type of the pairwise interaction has been represented by a numerical function,

$$f^m = \{f_1^m(r_1), f_2^m(r_2), \ldots f_k^m(r_K)\} \quad (3)$$

where r is the atom−atom separation that has been regularly spaced every 0.2 Å for separations ranging between 0 and 11.0 Å. Therefore, each type of interaction is described, in principle, by 55 f_k^m parameters, although some of those parameters for very short-range interactions cannot be determined due to the absence of the statistics because of the excluded volume interactions. The desired force field described by eq 3 has a linear dependence on the fitting parameters f_k^m, and therefore, the least-squares minimization of eq 2 can be reduced to the solution of an overdetermined system of linear equations.[49] Moreover, because the contribution to the virial (pressure) from the selected form

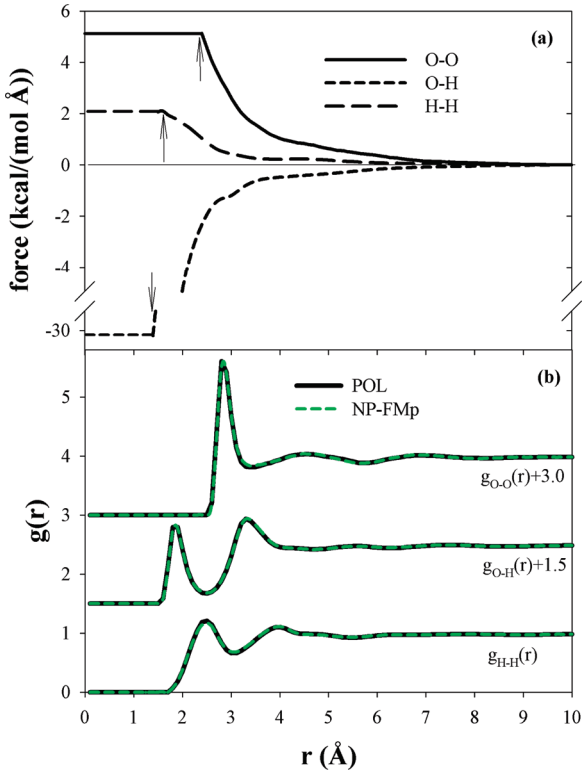

Figure 2. (a) Force profiles describing induced polarization interactions (induced dipole−induced dipole and charge-induced dipole) as a function of atom−atom separation for the NP-FMp model, as obtained using the FM approach for water. The r_c for each pairwise interaction type is indicated by arrows. (b) Radial distribution functions obtained from MD simulations of water at 298 K and atmospheric pressure using polarizable RPOL model and nonpolarizable NP-FMp model.

of fitting functions also has linear dependence on fitting parameters, it is easy using Lagrangian multipliers to impose a constraint that the fitted interactions would give a correct contribution to the pressure. In this work, we used the LU-decomposition method[67] to solve this system of equations. Finally, the fitted (every 500 fs) numerical functions f^n were averaged over 40 ps simulations. For each type of interaction, the corresponding energy dependence as a function of atoms separation was calculated using numerical integration of obtained f^n functions.

To validate our implementation of the FM methodology, we applied it to water, for which Iuchi et al.[48] have already investigated the possibility of approximating the many-body polarization interactions with two-body nonpolarizable potentials. For this purpose, MD simulations using the polarizable RPOL model were conducted at 298 K and atmospheric pressure (using a simulation protocol described in the next section), and the NP-FMp force field has been obtained according to the protocol described above. In Figure 2a, we show the resulting numerical potentials f^n. As can be seen, the numerical functions are smoothly approaching zero at large separations, indicating that the polarization interaction can be approximated using short-range interactions. However, for very short separations, the sampling during simulations with the polarizable force field was not available or had very limited sampling due to the dominance of van der Waals repulsive interactions, therefore resulting in noisy numerical functions for these separations (not shown). Following Iuchi et al, in this region, the force has been approximated as a constant with $f^n(r < r_c) = f^n(r_c)$, where r_c is the so-called "core" diameter which is indicated in Figure 2a by arrows for each type of interaction.

Subsequent simulation over 1 ns using the NP-FMp model resulted in radial distribution functions ($g(r)$) that are shown in Figure 2b, where they are compared with the corresponding $g(r)$ obtained from simulations using the RPOL model. Excellent agreement between simulations with the fitted NP-FMp and the original RPOL model can be seen. Simulations with the NP-FMp model predicted a density of 1001 kg/m^3 and a potential energy per molecule of −9.9 kcal/mol, which are in excellent agreement with those obtained from simulations using the RPOL model: a density of 1005 kg/m^3 and potential energy of −9.9 kcal/mol. The self-diffusion coefficient predicted by the NP-FMp model was 3.7×10^{-9} m^2/s, which is ∼45% higher than the value of 2.55×10^{-9} m^2/s obtained from simulations using RPOL model. Similar (42%) overestimation of the self-diffusion coefficient obtained from simulations using the force-matched nonpolarizable model and compared to the original TTM2-R polarizable model has been observed by Iuchi et al.[48]

Simulation Protocol. For all models and systems, MD simulations were conducted using the molecular simulation package Lucretius,[68] which has the capability to handle polarization effects. Covalent bond lengths were constrained using the velocity-Verlet form of the SHAKE algorithm.[69] The Ewald summation method was used for treatment of long-range electrostatic forces between partial charges and between partial charges and induced dipoles (for polarizable models). In simulations using polarizable models, a tapering function was used to drive the induced-dipole/induced-dipole interactions to zero at a cutoff of 11 Å, with scaling starting at 10 Å. Induced dipoles were calculated via a direct iteration with a predictor corrector method. A cutoff of 11 Å was used for all van der Waals interactions and the real part of electrostatic interactions in the Ewald summation. A multiple-time-step reversible reference system propagator algorithm[70] was employed; a time step of 0.5 fs was used for bonding, bending, dihedral, and out-of-plane deformation motions, a 1.5 fs was used for nonbonded interactions within a cutoff radius of 6.0 Å, and 3 fs was used for nonbonded interactions within the range of 6.0 and 11.0 Å and reciprocal part of electrostatic interactions. Each system was initially equilibrated in the NPT ensemble for at least 1 ns using integration scheme proposed by Martyana et al.[71] with frequencies of 0.01 fs^{-1} and 0.005 fs^{-1} for the thermostat and barostat control, respectively. Production runs ranged from 1 to 5 ns, depending on the system. The length of the production run was chosen to be long enough to allow molecules to reach a diffusive regime (mean squared displacement $\sim t$) and therefore allowing an accurate estimation of the self-diffusion coefficients.

The error estimation for properties obtained from our MD simulations has been performed the following way. For static properties such as density and heat of vaporization, simulation trajectories were divided into four equal subsets, and the property of interest was obtained for each of the subsets. Then a standard error analysis with 95% confidence limits was applied for the four independent measurements. For self-diffusion coefficients, the error bars were estimated from the variation of diffusion coefficients calculated for the x, y, and z directions using the entire trajectory available for each system. Since all systems investigated here are isotropic, the calculated one-dimensional self-diffusion coefficients should be the same and contribute 1/3 to the total self-diffusion coefficient. Hence, the variation in values of these one-dimensional coefficients can provide a good measure of the uncertainty of extracted self-diffusion coefficients. Error bars obtained these ways are reported in the corresponding tables or discussed in the text.

TABLE 2: Density (ρ) and Heat of Vaporization (ΔH_{vap},) Obtained from MD Simulations Using Polarizable (POL) and Nonpolarizable (NP) Force Fields at Specified Temperature and Atmospheric Pressure[a]

Material (N of mol. or ion pairs)	T, K	ρ, kg/m^3			ΔH_{vap} kJ/mol		
		POL	NP	$\delta\rho$, %	POL	NP	$\delta\Delta H_{vap}$, %
water (500)	298	1005	824	−17.9	43.9	28.3	−35.5
DMK (216)	298	776	736	−5.1	27.9	24.8	−11.2
EC (216)	313	1311	1256	−4.2	57.3	51.7	−9.7
[emim][BF_4]	298	1262	1259	−0.24	135.1	174.5	29.1
(150)	393	1196	1187	−0.75			
[emim][FSI]	298	1379	1371	−0.57	139.3	174.1	24.8
(125)	393	1312	1295	−1.30			
[emim][$N(CN)_2$]	298	1077	1059	−1.66	120.9	148.1	22.6
(180)	393	1018	1000	−1.78			
[bmmim][Ntf_2]	298	1411	1403	−0.59	128.0	152.7	19.4
(150)	393	1332	1318	−1.07			
[N_{1114}][Ntf_2]	298	1408	1397	−0.75	148.1	174.5	17.7
(150)	393	1325	1316	−0.71			
[pyr_{13}/][FSI]	298	1302	1290	−0.92	147.1	177.8	21.1
(216)	393	1233	1221	−0.97			

[a] Deviations δX is defined as $(X_{NP} - X_{POL})/X_{POL} \times 100$. Also specified is the number of molecules or ion pairs (N) used in MD simulations. Uncertainties for reported properties are less than 1.5 kg/m^2 for density and less than 0.5 kJ/mol for ΔH_{vap}.

III. Results and Discussion

A. Properties Predicted from MD Simulations Using POL and NP Models. ***Thermodynamic Properties.*** In Table 2 we report densities (ρ) and heat of vaporization (ΔH_{vap}) obtained from MD simulations using the POL and NP force fields at specified temperature and atmospheric pressure. For nonionic liquids, elimination of induced polarization effects results in significant (particularly for water) underestimation of density and heat of vaporization. The inability to induce additional dipoles in simulations with the NP force field results in the reduction of the average molecular dipole moments in these liquids, which in turn leads to lower density and ΔH_{vap} in liquids.

Table 2 also reports the density and ΔH_{vap} obtained from simulations using POL and NP force fields for six ILs. Similarly to nonionic liquids, turning off polarization results in density reduction for all ILs, albeit to a much smaller extent compared to the nonionic liquids. In ILs, the ionic interactions are much more dominant than the dipole−dipole interactions, and therefore, one can expect that the reduction of average molecular dipoles (due to elimination of induced dipoles in the NP model) would not significantly affect the strength of intermolecular interactions and, hence, will result in much smaller changes in density. Taking into account the reduction of average molecular dipole moments and density, one can also expect that ΔH_{vap} (defined as a heat required to evaporate an ion pair from a liquid phase) for the NP model would be smaller compared to simulations with the POL force field. However, Table 2 shows that upon turning off polarization interactions, ΔH_{vap} increases by about 20−30%, a trend qualitatively opposite to what we have observed for nonionic liquids. To understand this trend, it is instructive to compare average molecular dipoles in the liquid and gas phases from two force fields.

In Table 3, we report the average molecular dipoles obtained from simulations of [pyr_{13}][FSI] at 393 K using both models. Other ILs showed similar trends and, therefore, are not shown. For the NP force field, the molecular dipole moment (defined relative to the ion center of mass) is determined by the distribution of fixed partial atomic charges (the same for all four cases reported in Table 3) and population of molecular conformations. For [pyr_{13}][FSI], the latter is very similar in the gas and liquid phases, and therefore, the average molecular dipole moments reported in Table 3 obtained from simulations using the NP force field do not show any noticeable changes between the two phases. For the POL force field, an additional contribution from induced atomic dipoles should also be taken into account in the calculation of molecular dipoles. Table 3 shows that in the gas phase, the inclusion of polarization effects results in significantly larger (compared to the NP force field) molecular dipoles for both cation and anion. In the absence of any charge-screening environment, each ion induces a significant dipole moment on the counterion. However, in the liquid phase, the molecular dipole moments obtained from simulations with the POL force field are only slightly higher than those obtained from simulations with the NP force field. In the liquid, polarization between a pair of ions is compensated by polarization effects from other surrounding ions, resulting in partial cancellation of the polarization contribution to molecular dipoles. As a result, the strength of interaction between ions in the liquid phase obtained from simulations using POL and NP force fields is similar, as can be seen from Table 3, where the total energy per ion pair is reported for each case. The difference between the two force fields is only 3.7 kcal/mol, with the POL force field showing more favorable (stronger) interaction, whereas in the gas, the total energy per pair is 10.9 kcal/mol larger for the POL force field. This significantly stronger attraction for the cation−anion pair in the gas phase is the primary reason for the substantially smaller values of ΔH_{vap} reported in Table 2 for the POL force field as compared to NP.

TABLE 3: Average Molecular Dipole Moment in Debye and Total Energy per Ion Pair (E_{ip}) in kcal/mol, As Obtained from Liquid and Gas Phase[a] Simulations of [pyr_{13}][FSI] IL at 393 K and Atmospheric Pressure

	pyr_{13}	FSI	E_{ip}
NP (gas)	2.06	1.10	−46.0
NP (liquid)	2.11	0.86	−85.9
POL (gas)	2.83	3.12	−56.9
POL (liquid)	2.21	1.34	−89.6

[a] The gas phase simulations were performed for cation−anion pairs.

Dynamic Properties. To obtain the self-diffusion coefficient, a mean-squared displacement (MSD) for each molecule type was calculated as a function of time (t). The self-diffusion coefficients were obtained from fitting the MSD(t) as a linear function of t (MSD(t) $\sim 6Dt$) for data where MSD(t) > 10.0 Å^2. The latter condition ensures that the fitting is done for time

TABLE 4: Self-Diffusion Coefficients (D, in 10^{-10} m^2/s) Obtained from MD Simulations Using Polarizable (POL) and Nonpolarizable (NP) Force Fields[a]

material	T (K)	POL	NP	D_{POL}/D_{NP}	POL	NP	D_{POL}/D_{NP}
water	298	2.55	13.6	0.19			
DMK	298	4.55	5.2	0.88			
EC	313	0.78	0.96	0.81			
		Cation			Anion		
[emim][BF_4]	298	0.48	0.12	4.0	0.36	0.12	3.0
	393	3.95	2.09	1.9	3.34	1.52	2.4
[emim][FSI]	298	0.76	0.21	3.6	0.68	0.21	3.2
	393	4.20	2.58	1.6	3.85	2.11	1.8
[emim][$N(CN)_2$]	298	0.91	0.46	2.0	1.08	0.47	2.3
	393	6.63	3.87	1.7	6.90	4.51	1.5
[bmmim][Ntf_2]	298	0.22			0.18		
	393	2.68	1.24	2.2	2.33	0.87	2.7
[N_{1114}/][Ntf_2]	298	0.12			0.11		
	393	1.96	0.71	2.8	1.61	0.87	1.9
[pyr_{13}][FSI]	298	0.18			0.20		
	393	1.85	0.62	3.0	2.20	0.84	2.6

[a] Also shown is the ratio of self-diffusion coefficients, D_{POL}/D_{NP}, obtained from simulations using polarizable and nonpolarizable force fields. Uncertainty of reported self-diffusion coefficients is <10%.

scales on which ion motion is diffusive. Table 4 reports self-diffusion coefficients obtained from simulations using POL and NP force fields as well as their ratio. For nonionic liquids, the relatively weaker intermolecular interactions (manifested in ΔH_{vap}) and lower liquid density predicted by the NP model also lead to a faster dynamics in these systems, as indicated by less than unity ratios of D_{POL}/D_{NP} reported in Table 4. Unlike water, for which the ratio between self-diffusion coefficients obtained from the NP and POL models is almost factor of 5, for EC and DMK, the NP model predicts dynamics within 20% from results obtained using the POL model. This is consistent with the much better agreement of densities and ΔH_{vap} obtained for these liquids from simulations using the POL and NP models (Table 2), as compared to that for water. It also indicates that polarization interactions in the RPOL water model play a much more important role than in EC and DMK, despite the fact that all those molecules have large dipole moments. Such exceptional behavior of water is likely a consequence of strongly correlated local water structure (due to the hydrogen bonding network) which allows (a) relatively close atom−atom approaches and (b) intermolecular alignment of permanent dipoles, both of which enhance induced polarization interactions.

For ILs, an opposite effect as compared to nonionic liquids is observed; despite a slight reduction in density, the dynamics obtained from simulations using the NP force field are significantly slower (D_{POL}/D_{NP} ranging from 1.5 to as much as 4.0) than those obtained with the POL force field. Our previous study has shown a correlation between ΔH_{vap} and ion dynamics.[72] In principle, the faster dynamics predicted by the POL model is consistent with the lower ΔH_{vap} obtained for this model as compared to the NP force field. On the other hand, we have explained above that the smaller values of the ΔH_{vap} are primarily due to stronger ionic pair interaction in the gas phase predicted by the POL force field, whereas in the liquid phase, the energies per ion pair obtained from two force fields are similar, with the POL force field predicting a slightly stronger interaction. This apparent contradiction further illustrates that correlations between thermodynamic and transport properties might be more complex than the simple relations such as suggested in ref 72. Table 4 also shows that the D_{POL}/D_{NP} has noticeable temperature dependence. For three ILs for which the self-diffusion coefficients were calculated at 298 and 393 K, D_{POL}/D_{NP} significantly increases as the temperature decreases. This indicates that turning off polarization not only results in systematic slowing down of ion translational motion but also changes its temperature dependence. Hence, if Arrhenius behavior is assumed for self-diffusion coefficients, then the corresponding activation energies obtained from simulations using POL and NP models will be different. Finally, we would like to point out that self-diffusion coefficients predicted for [emim][BF_4], [bmmim][Ntf_2], and [N_{1114}][Ntf_2] using the POL model are in excellent agreement (within less than 20% deviation) with available experimental data.[47]

The observed slowing down of ion mobility in simulations using the NP force field is consistent with other simulation works[28,29,31,34,44] discussed above that applied nonpolarizable force fields for modeling of various ILs and reported systematic significant underestimation of ion mobility and other transport properties as compared to experiments. Taking into account that for ILs investigated here, the POL model predicts self-diffusion coefficients within 20% from the available experimental data,[47] values obtained using our NP model are within a factor of 2−4 from the experimental data, which is still better than many predictions reported in the literature. Importantly, the observed slowing down predicted by the NP model also diminishes the computational efficiency of the nonpolarizable model as compared to the polarizable. As we pointed out in the Introduction, simulations with polarizable models are a factor of 3−4 computationally more expensive than with nonpolarizable force fields. However, if nonpolarizable models predict a factor of 2−4 slower dynamics, then accessing the same extent of structural relaxation (characterized by molecular displacements) with the nonpolarizable force field would require 2−4 times longer trajectories than those with polarizable force field that predict much more realistic dynamics. Hence, the net computational expenses are almost equivalent for the POL and NP models, albeit more accurate dynamics are predicted using the POL model.

We also investigated the influence of polarization on ion rotational dynamics. For each molecule, a local coordinate system has been defined, and a rotational autocorrelation function (ACF) for each unit vector $\mathbf{e}_i$ ($i = \{x, y, z\}$) defining this local coordinate system has been calculated as

$$\mathrm{ACF}_i(t) = \langle [\mathbf{e}_i(0) \cdot \mathbf{e}_i(t)] \rangle \quad (4)$$

where $\mathbf{e}_i(0)$ and $\mathbf{e}_i(t)$ are the values of the unit vectors at time zero and t, respectively, and brackets denote the ensemble average over all molecules of the same type and time origins. The location of the origin and orientation of selected local coordinate systems for each molecule are given in the Supporting Information. For the N_{1114} cation, a vector between the nitrogen atom and the methyl carbon on the butyl tail was considered instead of the rotation of the local coordinate system. Due to the symmetric structure of BF_4, the rotation around all axes are equivalent. The obtained ACFs were fitted with Kohlrausch−Williams−Watts (KWW) functions given by

$$P_{KWW}(t) = A \exp(-(t/t_r)^{\beta}) \quad (5)$$

where t_r is a relaxation time parameter, parameter β determines the degree of stretching and characterizes the broadness of the relaxation process, and prefactor A allows us to account for decay that occurs on time scales faster than 1 ps^{-1}. Rotational relaxation times (τ) were obtained by integrating eq 5 over time

TABLE 5: Rotational Relaxation Time τ (ps) Obtained from MD Simulations at 393 K using POL, NP, and NP-FMe Force Fields[a]

	cation			anion		
	τ_x	τ_y	τ_z	τ_x	τ_y	τ_z
[emim][BF_4], POL	48.1	20.9	22.4	1.3		
[emim][BF_4], NP	78.2	28.4	31.0	1.6		
[emim][BF_4], NP-FMe	99.0	30.5	31.4	1.1		
τ_{NP}/τ_{POL}	1.63	1.36	1.38	1.20		
$\tau_{NP\text{-}FMe}/\tau_{POL}$	2.06	1.46	1.40	0.85		
[emim][FSI], POL	39.7	14.6	16.5	13.3	4.0	4.2
[emim][FSI], NP	55.1	18.0	21.2	18.8	4.5	4.3
[emim][FSI], NP-FMe	47.3	16.1	17.6	15.8	4.2	3.9
τ_{NP}/τ_{POL}	1.39	1.24	1.29	1.41	1.12	1.02
$\tau_{NP\text{-}FMe}/\tau_{POL}$	1.19	1.10	1.07	1.19	1.04	0.92
[pyr_{13}][FSI], POL	18.7	50.6	29.9	18.3	5.6	4.8
[pyr_{13}][FSI], NP	22.1	87.9	41.6	32.8	6.2	5.9
[pyr_{13}][FSI], NP-FMe	17.8	62.0	30.8	21.4	5.3	4.9
τ_{NP}/τ_{POL}	1.18	1.74	1.39	1.79	1.11	1.22
$\tau_{NP\text{-}FMe}/\tau_{POL}$	0.95	1.23	1.03	1.17	0.96	1.02
[emim][dca], POL	34.9	14.8	16.6	17.1	1.29	1.20
[emim][dca], NP	46.9	17.6	21.1	24.4	1.51	1.41
τ_{NP}/τ_{POL}	1.35	1.19	1.27	1.43	1.17	1.17
[bmmim][Ntf_2], POL	61.3	78.1	57.2	50.7	12.8	16.1
[bmmim][Ntf_2], NP	97.8	131.2	84.6	81.8	16.7	18.9
τ_{NP}/τ_{POL}	1.59	1.68	1.48	1.61	1.30	1.17
[N_{1114}][Ntf_2], POL	97.6			62.1	14.9	21.4
[N_{1114}][Ntf_2], NP	192.0			126.3	22.0	26.3
τ_{NP}/τ_{POL}	1.97			2.03	1.47	1.23

[a] Also shown are the ratios of rotational relaxation times.

from zero to infinity and are given in Table 5 for all ILs at 393 K. This Table shows that slowing down of rotational dynamics upon turning off polarization is significantly less pronounced than what was observed for translational motion characterized by the ion self-diffusion coefficients (Table 4). For example, in [emim][BF_4], simulation with the NP force field translational motion of BF_4 is ~2.4 times slower than in simulations with the POL model, yet the rotational dynamics obtained from simulations with the NP force field is only 20% slower. Interestingly, for all ions (for which the three distinct relaxation times were defined), the rotation around the axis with the smallest relaxation time is the least influenced by turning off the polarization. These results are consistent with the decoupling of the PF_6^- rotation from its diffusion observed in prvious simulations of [bmim][PF_6].[46]

Structural Correlations. As we discussed above, the observed difference in dynamics of ILs predicted from simulations using POL and NP force fields does not correlate well with thermodynamic properties obtained from simulations with these force fields. Therefore, hoping to find explanations for observed differences in dynamical properties, we next examined the difference in structural correlations obtained from simulations of ILs using these force fields. For this purpose, we are focusing on the analysis of molecular structure. Although it is also possible to examine atom−atom correlations, this is outside the scope of the current paper. Figure 3 shows cation/cation, cation/anion, and anion/anion center-of-mass radial distribution functions ($g(r)$) for [emim][BF_4], [emim][FSI], and [pyr_{13}][FSI] liquids at 393 K and atmospheric pressure. For almost all correlations, the peaks in $g(r)$ obtained from simulations using the NP model are narrower and higher as compared to those obtained using the POL model, indicating that systems modeled with the NP force field show more structuring or stronger spatial correlations between ions. The latter is typically a consequence of stronger intermolecular interactions;[73] however, as we showed above, the energy per ion pair in the liquid phase predicted by the NP model is actually smaller than the one obtained using the POL force field. Comparison of molecular center-of-mass $g(r)$ obtained from simulations using POL and NP force fields for nonionic liquids (EC and DMK) showed very minor differences (not shown in the figure), most of which are a direct consequence of changes in the density predicted by the two force fields. No noticeable enhancement of structuring upon turning off the polarization has been observed in these nonionic liquids. Therefore, as in the case of dynamics, the observed enhanced structuring of ILs in simulations with the NP force field is unexpected.

We further examine the difference in structure predicted from simulations using NP and POL force fields by comparing 3-dimensional (3-D) density distributions of selected anion atoms around a cation. In Figure 4, we show isosurfaces for distribution of the BF_4 boron atoms around the emim cation. In this analysis, the center of the local coordinate system is located on the emim sp^2 carbon bonded to two nitrogen atoms, and the N−C−N bend defines one of the coordinate system planes. The simulation box is divided into lattice cells of size 1.0 Å, and the relative density distribution $\rho_i/\langle\rho\rangle$, where ρ_i is the local density of boron atoms in the ith lattice cell and $\langle\rho\rangle$ is the average density of boron atoms in the system, is calculated by averaging over all emim molecules and the entire trajectory. Locations around the cation corresponding to the lower free energy of boron atoms will be more populated and, hence, will have larger values for the calculated relative density. The maximum values of $\rho_i/\langle\rho\rangle$ were 21.1 and 21.7 for simulations with POL and NP force fields, respectively.

Figure 4 compares several representative isosurfaces with $\rho_i/\langle\rho\rangle = 6.0$, 10.0, and 14.0. For the higher free energy isosurface ($\rho_i/\langle\rho\rangle = 6.0$), simulations with the POL provide a continuous path above the N−C−N bend from one side of emim to another, and simulations with the NP force field have two disconnected isosurfaces. This indicates that the NP force field results in a larger free energy barrier for the BF_4 to move from one side of emim to another. For $\rho_i/\langle\rho\rangle = 10.0$, the isosurfaces between two force fields are very similar, with the NP having a slightly larger area for the two upper regions. However, for the lower free energy isosurface, $\rho_i/\langle\rho\rangle = 14.0$, a pronounced difference between force fields can be seen. The POL model predicts that only two regions under the emim molecule are populated for this isosurface, and two upper regions have disappeared, indicating that the two upper probable locations of boron atoms have a higher free energy as compared to the two lower regions. The NP model, on the other hand, predicts that all four regions are basically equivalent and well-populated, as indicated by the significant area of the isosurfaces in the upper regions. This means that instead of two deep and two shallow free energy locations of boron atoms around the emim, as predicted by the POL model, the NP model predicts four deep free energy locations. These results indicate that the POL model provides more asymmetric interaction of ions in the bulk IL, as compared to the NP model. Similar behavior is observed for other ILs.

It is tempting to correlate the observed differences in 3-D distributions in Figure 4 with differences in dynamics predicted from simulations using these force fields. Indeed, the continuous path observed for the higher free energy (low density) isosurface should facilitate the mobility of BF_4 around the emim molecule for the POL model, while in the NP model the boron atom would need to overcome a larger free energy barrier to cross from one side of the molecule to another which certainly can

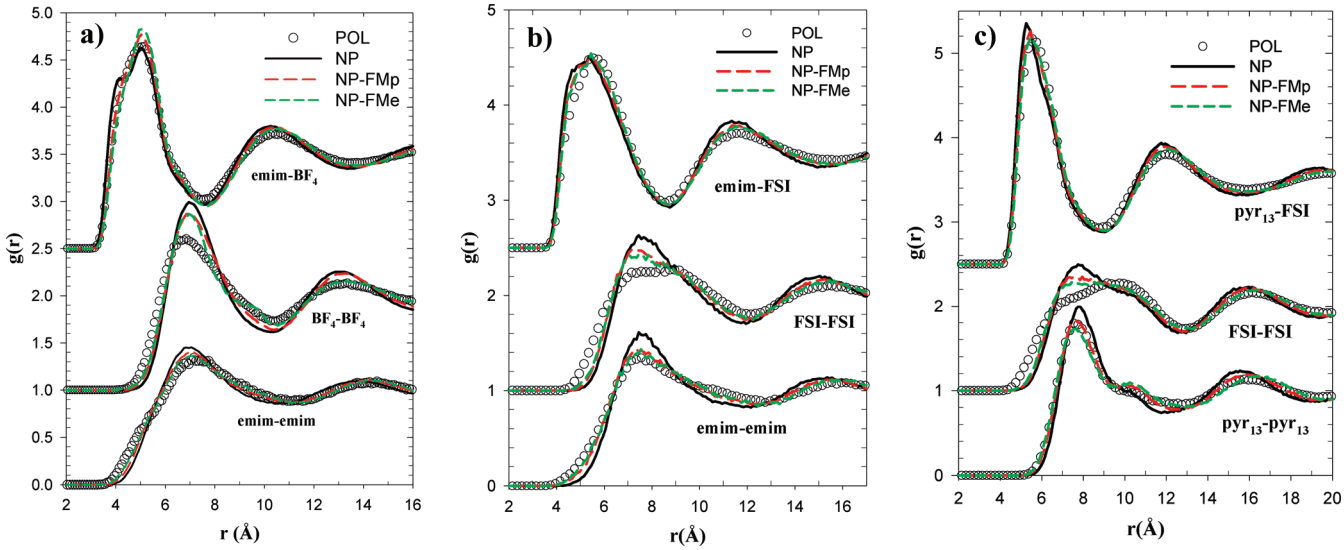

Figure 3. Molecular center-of-mass cation−cation, cation−anion, and anion−anion radial distribution functions ($g(r)$) obtained from simulations using four different force fields for [emim][BF_4] (a), [emim][FSI] (b), and [pyr_{13}][FSI] (c) at atmospheric pressure and 393 K.

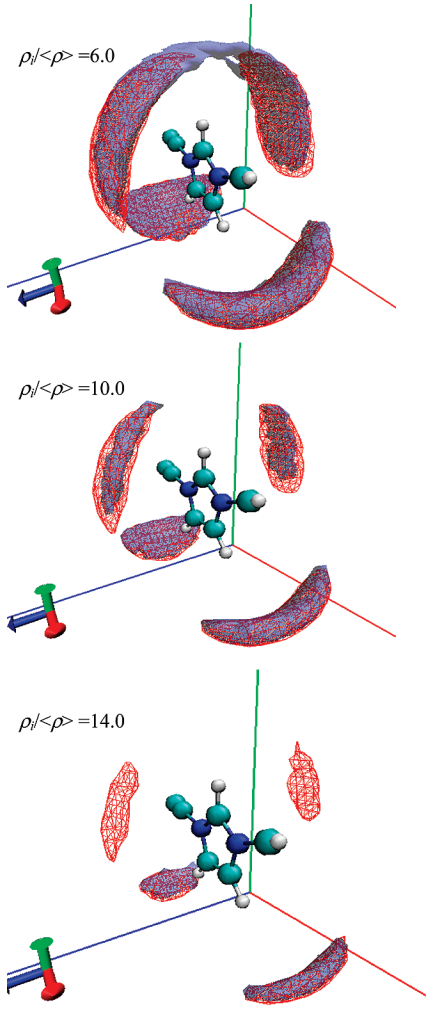

Figure 4. Isosurfaces of 3-D density distribution of BF_4 boron atoms around emim molecule (see text for details) obtained from simulations at 393 K using POL (solid gray) and NP (red wireframe) models.

restrict the mobility of BF_4 around emim. Also having four locations with deep free energy minima (instead of two deep and two shallow as in the POL model) can slow down mobility of BF_4 around the emim as well as from one emim molecule to another in simulations with the NP model. While these sup-

TABLE 6: χ^2 Deviations between Forces Obtained from POL and Nonpolarizable Force Field on the Same Configurations of ILs[a]

	NP	NP-FMp	NP-FMe
[emim][BF_4]	0.37	0.15	0.19
[emim][FSI]	0.22	0.06	0.08
[pyr_{13}][FSI]	0.3	0.09	0.11

[a] χ^2 is in units of kcal/(mol Å)^2.

positions appear to be quite reasonable and have been suggested previously in the literature,[54] below we show that observed differences in the 3-D distributions cannot explain the slowing down of ion dynamics upon turning off polarization.

B. Simulations Using NP-FM Models. ***Quality of Fits.*** To characterize the improvement provided by the newly fitted numerical NP-FM potentials, we have compared χ^2 defined in eq 2 for each nonpolarizable force field. For several configurations generated from simulations with the POL force field, forces on each atom have been computed using each nonpolarizable model (NP, NP-FMp, NP-FMe) and then compared with the corresponding forces obtained using the POL model. Table 6 reports averaged (over all atoms) χ^2's for the three IL systems investigated. In the NP model, no two-body interactions have been fitted/added, and therefore, χ^2 represents the average magnitude (squared) of force components (x, y, and z) due to polarization interactions (induced dipole−induced dipole and induced dipole−charge) per atom. Note that the average (over all atoms) magnitude of the force components (x, y, or z) due to all nonbonded interactions (van der Waals and electrostatic) is ∼2.0 kcal/mol/Å for the three ILs investigated. Therefore, contribution to the total nonbonded force from polarization interactions is on the order of 20−30%.

As can be seen from Table 6, both NP-FM models provide significant improvement in reproducing forces obtained from the POL model as compared to the NP model. The NP-FMe model has a slightly larger χ^2 than the NP-FMp. On the one hand a larger χ^2 can be anticipated for this model because it fits all electrostatic forces (including charge−charge interactions) whose magnitude is noticeably larger than the forces just due to polarization interactions fitted by the NP-FMp model. On the other hand, the NP-FMe model has additional flexibility of manipulating with all electrostatic interactions and potentially

could redistribute forces between different types of pairwise interactions to minimize χ^2. The latter is particularly important in light of the following arguments. One can argue that for a nonpolarizable model, a set of partial atomic charges different from those used in the polarizable force field would be more appropriate and would provide a better description of the electrostatic field around the molecules as well as molecular dipoles and quadrupoles. Hence, the NP-FMp model, which only fits contribution to forces from polarization interactions while keeping partial atomic charges the same as in the POL model, might not provide the best description of total forces acting on each atom. The NP-FMe model, on the other hand, is not constrained to have the same charges as in the POL model (all electrostatic interactions are fitted by numerical potentials) and, therefore, can have a set of numerical potentials that effectively represent any distribution of the partial atomic charges that minimizes χ^2. However, as we can see from Table 6, this extra flexibility of the NP-FMe model does not result in further improvement in the description of the forces from the POL model.

Structural Properties. To determine whether the improved force description in the NP-FM models has any influence on structural and dynamical properties of ILs, we have compared them with the already discussed above predictions from the POL and NP models. First, the 3-D distributions of boron atoms around emim in the [emim][BF_4] system as obtained from simulations using POL and NP-FMe models are compared in Figure 5. Unlike the NP model, which showed isosurfaces significantly different from those obtained using the POL model, distributions from the NP-FMe and POL models are in very good agreement. For the higher free energy isosurface ($\rho_i/\langle\rho\rangle = 6.0$), the NP-FMe model provides a similar continuous path from one side of the N−C−N bend to the other, whereas for the lower free energy isosurface ($\rho_i/\langle\rho\rangle = 14.0$), the NP-FMe model shows only two populated areas, again in excellent agreement with predictions by the POL model. A similar improvement in local 3-D distributions has been observed in [emim][FSI] and [pyr_{13}][FSI] systems for both NP-FM models (not shown). This clearly illustrates that a better reproduction of forces from the POL model by the NP-FM models significantly improves local cation/anion distributions.

On the other hand, examination of Figure 3, in which the cation/anion center-of-mass $g(r)$ obtained from simulations using NP-FM models are compared with those obtained from POL and NP models, indicates that although the NP-FM models show a better agreement with the POL than the NP model, they still have a noticeable mismatch with the $g(r)$ from the POL model. Interestingly, for all three systems, the cation−cation and cation−anion $g(r)$ obtained using NP-FM models are in very good agreement with predictions of the POL model, consistent with the improved 3-D distributions shown in Figure 5. Yet, the anion−anion distributions show significant deviations for all investigated ILs. These deviations indicate that although NP-FM models can significantly improve local cation−anion and cation−cation correlations, they are still missing some effects influencing the anion−anion distributions.

Dynamic Properties. We also compared dynamics obtained from simulations using the NP-FM models with those predicted using the POL and NP models. Figure 6 shows cation and anion self-diffusion coefficients for three ILs investigated obtained from simulations using all four models. For [emim][FSI] and [pyr_{13}][FSI] ILs, the use of NP-FM models noticeably improves the agreement with the POL model predictions for both ions, with the NP-FMe model giving a somewhat better agreement

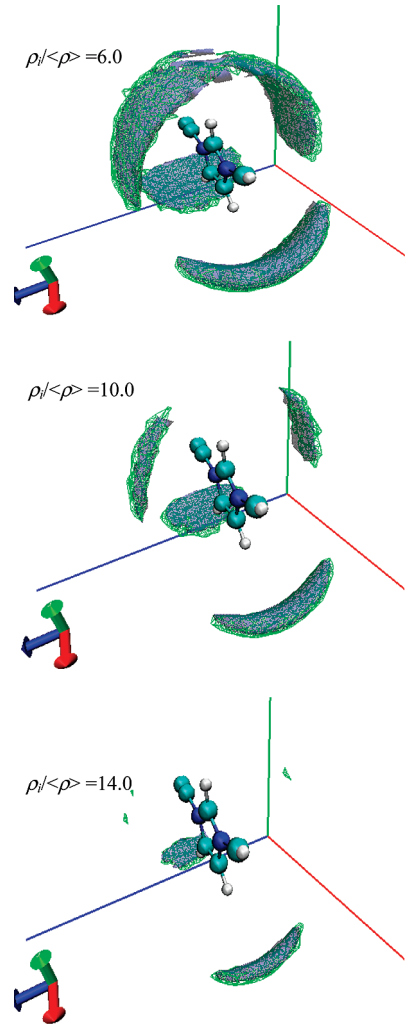

Figure 5. Isosurfaces of 3-D density distribution of BF_4 boron atoms around the emim molecule (see text for details) obtained from simulations at 393 K using POL (solid gray) and NP-FMe (lime wireframe) models.

than the NP-FMp model. For these systems, the use of FM fitted potentials allowed us to reduce by almost 50% the discrepancy observed between mobilities predicted from the POL and NP models, although deviations are still noticeable. However, for the [emim][BF_4] system, despite observed significant improvement in the description of structural correlations, simulations with NP-FM models did not provide any noticeable speed-up for either of the ions such that it would improve the agreement with predictions from the POL model. The lack of improvement in description of ion mobilities with NP-FM models for the [emim][BF_4] is somewhat puzzling. The extent of the deviations/improvement in pair distribution functions between simulations with POL and NP-FM models (Figure 3) are basically the same for all three systems. In addition, as we show in Figure 5, the local distribution of BF_4 around emim has significantly improved in simulations with the NP-FMe model. Yet, all these improvements in description of structural correlations do not appear to influence the description of the dynamical properties. We also found that the degree of uncorrelated ion motion[47] is independent of the force field used, and therefore, we expect that ionic conductivities of these systems will follow the same trend as obtained self-diffusion coefficients.

To further understand the influence of different potentials on translational dynamics, we have examined the time dependence of the ions' center-of-mass mean squared displacement (MSD)

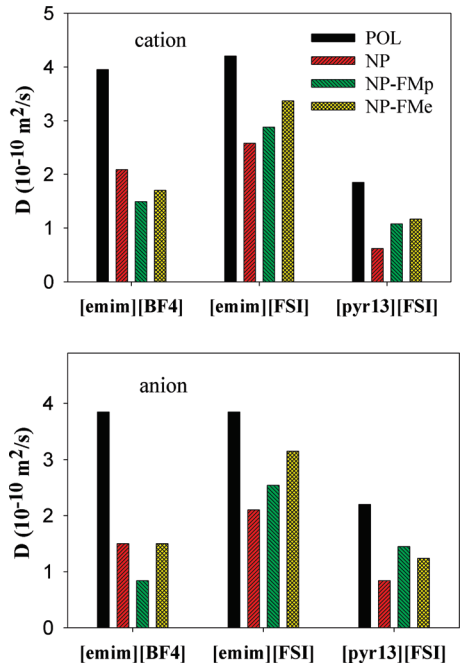

Figure 6. Cation and anion self-diffusion coefficients as obtained from simulations at 393 K using POL, NP, and NP-FM models.

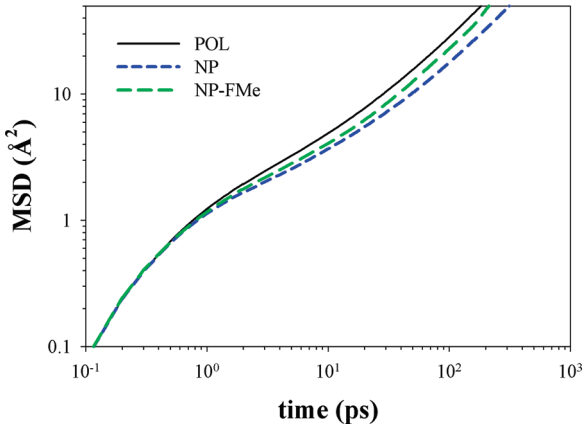

Figure 7. Mean-squared displacement of emim center of mass in the [emim][FSI] as a function of time as obtained from MD simulations using the POL, NP, and NP-FMe models at 393 K.

and velocity autocorrelation function (VACF) obtained from simulations using different models. In Figure 7, the MSD of emim cation is shown as a function of time as obtained from MD simulations of [emim][FSI] at 393K using the POL, NP and NP-FMe models. For time scales less than 500 fs, there is basically no dependence of the ion mobility on the employed force field. This time scale corresponds to a motion in the cage formed by the first coordination shell. However, at longer time scales, the nonpolarizable models begin to show deviations from the POL model whose MSD becomes systematically larger at a given time scale. Examination of Figure 8, where the VACF for the emim center-of-mass is shown for the same system and conditions, shows that on a time scale of 500 fs, the emim VACF has one oscillation that can be roughly attributed to a single collision. For times less than 500 fs, the VACF obtained from simulations using different force fields also match very well. However, at longer times, we can see that simulations with the POL model results in a faster damping of the VACF, as compared to nonpolarizable models, consistent with the Hansen and McDonald explanation[55] discussed in the Introduction. At longer time scales, the MSD(t) and VACF(t) obtained from

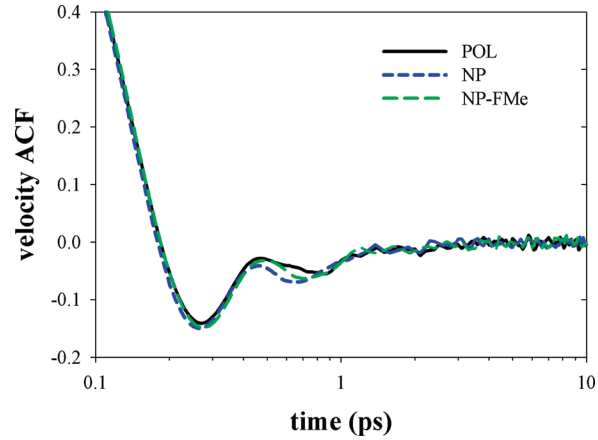

Figure 8. Normalized (by average velocity squared) velocity autocorrelation function (VACF) of emim center-of-mass in the [emim][FSI] as a function of time, as obtained from MD simulations using the POL, NP, and NP-FMe models at 393 K.

simulations using NP-FMe model are in better agreement with the predictions using the POL model than those obtained from the NP model, which is consistent with self-diffusion coefficients reported for this system in Table 4.

We also examined the influence of the NP-FM models on rotational dynamics. Table 5 shows that with the exception of [emim][BF_4], simulations with the NP-FMe model provide noticeable improvement (as compared to the NP model) in the description of rotational dynamics of cations and anions predicted using the POL model, although as we pointed out above, the discrepancies between the POL and NP models for rotational dynamics were not as pronounced as for translational motion. This is further illustrated in Figure 9, where rotational ACFs are shown as a function of time for the emim cation in [emim][FSI] at 393 K as obtained from simulations using different force fields. ACF for rotation around each axis of the selected local coordinate system (also defined in Figure 9) shows independence of the force field employed up to an ~3 ps time scale, after which ACFs obtained from simulations using the POL model show systematically faster relaxation. However, simulations with the NP-FMe model show rotational relaxations very similar to those obtained from using the POL model.

Force Fluctuations. Perhaps some insight into why prediction of dynamic properties using nonpolarizable models is challenging for most investigated ILs and why an improved description of structural correlations does not transfer into improved dynamics (at least for some ILs studied here) can be obtained from an analysis of fluctuations of forces acting on atoms. We have calculated the distribution of the magnitude of the total nonbonded force for the selected type of atoms using different force fields. In Figure 10, these distributions are shown for the FSI nitrogen in [emim][FSI] at 393 K using POL, NP and NP-FMe force fields. First, we calculated these distributions using exactly the same configurations generated in simulations with the POL force field (those are shown as symbols in Figure 10). Note that the same configurations were used to fit the NP-FMe model in the FM approach. As we can see, the NP and POL distributions are noticeably different, with the former being broader and shifted to larger values. On the other hand, distribution for the NP-FMe model lies basically on top of the POL model distribution, indicating that the fitted NP-FMe model does a very good job in reproducing not only the average force but also the distribution of force magnitude acting on a given atom type. However, if the same distributions are calculated from simulations with the corresponding nonpolarizable force

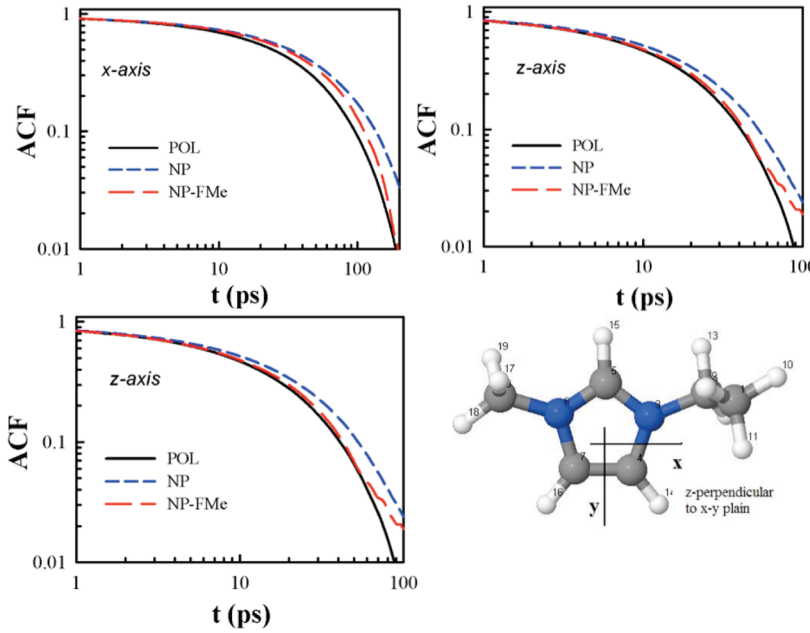

Figure 9. Rotational ACF of emim around each axis of the selected local coordinate system (schematically illustrated on the lower right) as a function of time as obtained from simulations of [emim][FSI] using the POL, NP, and NP-FMe models at 393 K.

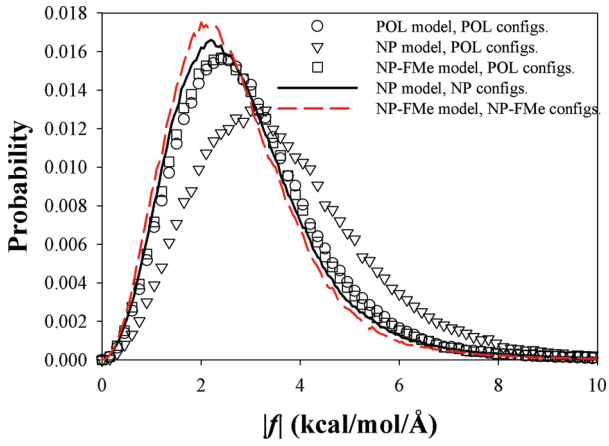

Figure 10. Probability distribution of the magnitude of the total nonbonded force acting on an FSI nitrogen in the [emim][FSI] at 393 K obtained using different models (see text for details).

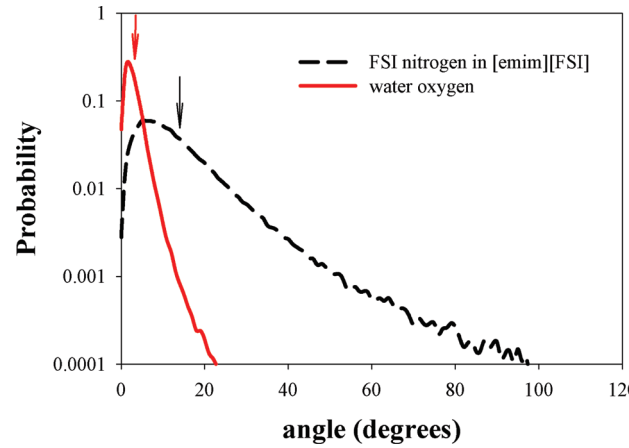

Figure 11. Distribution of angles between the total nonbonded forces predicted from the POL and NP-FMp models and acting on the FSI nitrogen in [emim][FSI] at 393 K and water oxygen in pure water at 298 K. Forces from both force fields were calculated using the same system configurations generated using the POL model. Vertical arrows show the average angle for each distribution (14.05 for [emim][FSI] and 2.81 for water).

field (i.e., distribution of NP-FMe forces are calculated from simulations using the NP-FMe model), then noticeably different distributions (solid lines) can be observed in Figure 10.

Distributions of forces obtained from simulations using NP and NP-FMe force fields are narrower than those obtained from the POL model and are shifted to lower values. This indicates that while the NP-FMe model provides a good description of POL forces for configurations generated with the POL model, when the system is simulated with the fitted NP-FMe force field, it is capable of relaxing into a somewhat different structure (as can be clearly seen in the pair correlations functions shown in Figure 3) and reducing the magnitude of forces acting on individual atoms. A similar effect is seen for all atom types and other systems.

To understand how the NP-FMe model on one hand can accurately reproduce distribution of forces predicted by POL model for configurations generated using POL model, yet on the other hand not be able to maintain the same structure in simulations when the NP-FMe force field is employed, we have analyzed the ability of the fitted model to capture directionality of forces acting on a specific atom in a given configuration. In this analysis, we took a set of system configurations (generated using POL model) and for each atom type calculated components of the force vector (only forces due to nonbonded interactions) predicted with the POL and NP-FM models. For each atom in every configuration, the angle between force vectors predicted using the POL and NP-FM force fields have been determined. If NP-FM models could accurately reproduce the directionality of the forces obtained from the target POL model, then the angle would be small or zero. In Figure 11, we show a probability distribution of those angles for the FSI nitrogen in the [emim][FSI] system at 393 K. As we can see, the distribution is relatively broad, with a significant fraction of occurrences when the angle is larger than 20°, indicating that, in this specific case, the NP-FMp model cannot capture exactly the directionality of the nonbonded forces predicted by the POL model. Since forces due to van der Waals and Coulomb (fixed partial charges) interactions are the same in the NP-FMp and POL models, the observed mismatch in forces directionality

is due to the inability of fitted two-body interactions to capture all the nuances of many-body polarization interactions. As a result, when systems are allowed to evolve using fitted nonpolarizable model (i.e. NP-FMp or NP-FMe), they are driven to different, energetically more favorable configurations corresponding to the selected nonpolarizable model. However, it is practically impossible to determine whether the observed difference in dynamics between the POL and NP-FM models is a direct consequence of differences in the underlying structure predicted by these force fields or a result of variations in the directionality and magnitudes of instantaneous forces on individual atoms. Results from simulations of simple molten salts,[51] for which inclusion of polarization had no discernible effect on the structure yet resulted in an increased ion mobility, seem to be supporting the latter argument, although the difference in dynamics predicted in that work using polarizable and nonpolarizable force fields was significantly smaller (~10−20%) as compared to what we observe for room temperature ILs investigated here (a factor of 1.5−4.0).

Finally, although for all three ILs, we found that neither of the NP-FM models can reproduce the structure or dynamics obtained from simulations using the POL model in section II, we showed that the FM approach worked very well for water, at least in reproducing the structure and thermodynamics. Radial distribution functions obtained using the NP-FMp model were in excellent agreement with those obtained from the POL model. Analysis of fluctuations in the forces' magnitude and directionality similar to that discussed above for the ILs revealed that the FM approach for water shows very different results. For comparison, in Figure 11, we also show the distribution of angles between forces predicted from POL and NP-FMp models for the same configurations (generated using the POL model) and acting on water oxygen atoms. As we can see, the distribution is very narrow, with the most probable angle <2° and practically no probability of finding angles larger than 20°. We speculate that the strong hydrogen-bonding network in water somehow influences the orientation of forces due to many-body polarization such that those forces can be easily represented/decomposed between available (for a given configuration) pairwise interactions. Investigation of the ability of the FM approach to obtain two-body potentials that can accurately reproduce forces due to many-body polarization interactions is currently ongoing for a wide class of ionic and nonionic materials and will be reported in our future publication.

IV. Conclusions

In our previous studies, we demonstrated that MD simulations using the polarizable APPLE&P force field provide excellent predictions of thermophysical and dynamical properties for a wide variety of ILs. Here, we systematically investigate the influence of polarization interactions on structural, thermodynamic, and dynamic properties of several ILs. We showed that turning off polarization effects in ILs results in a 20−30% increase in the enthalpy of vaporization and a factor of 2−4 slowing down in translational dynamics as compared to results from simulations using the polarizable force field. These results are contrary to what is observed for nonionic liquids, for which turning off polarization resulted in a reduction in the enthalpy of vaporization and a speeding up of translational dynamics. Simulations of ILs using the nonpolarizable version of the APPLE&P force field also showed stronger correlations in ion−ion distribution functions. Interestingly, the slowing down of ion rotational dynamics upon turning off polarization interactions was significantly less pronounced as compared to that seen for translational dynamics. Although properties predicted from simulations using the nonpolarizable version of the APPLE&P force field clearly show significant deviations from experimental data, they are quite reasonable when compared to many other predictions reported in the literature from MD simulations of ILs using nonpolarizable models. For example, slower (than in experiment) by a factor of 2−4 ion dynamics obtained in our work is significantly better than an order of magnitude deviations between experiments and simulations reported previously for various ILs in the literature.

Using the Force Matching approach, we also attempted to obtain two-body interactions that would effectively approximate forces from many-body polarization effects in the simulated ILs. We found that although the simulations with such fitted nonpolarizable potentials provide some improvement in reproducing structural and dynamical properties obtained from simulations with the polarizable force field, this attempt to systematically represent many-body interactions with a numerical two-body potential did not provide dramatic improvements in structure and dynamics. We attribute this failure to the inability of two-body interactions to capture correctly the directionality of many-body polarization forces acting on each atom for a given configuration and the fluctuations of this directionality with changing configuration of the system.

Acknowledgment. The authors are grateful for financial support of this work by the Air Force Office of Scientific Research, Department of the Air Force Contract FA9550-09-C-0110 to Wasatch Molecular Inc. and the University of Utah. Opinions, interpretations, conclusions, and recommendations are those of the authors and are not necessarily endorsed by the United States Air Force. An allocation of computer time from the Center for High Performance Computing at the University of Utah is gratefully acknowledged.

Supporting Information Available: Additional information as noted in text. This material is available free of charge via the Internet at http://pubs.acs.org.

References and Notes

(1) Forsyth, S. A.; Pringle, J. M.; MacFarlane, D. R. *Aust. J. Chem.* **2004**, *57*, 113–119.
(2) Jin, C. M.; Ye, C. F.; Phillips, B. S.; Zabinski, J. S.; Liu, X. Q.; Liu, W. M.; Shreeve, J. M. *J. Mater. Chem.* **2006**, *16*, 1529–1535.
(3) Zeng, Z.; Phillips, B. S.; Xiao, J. C.; Shreeve, J. M. *Chem. Mater.* **2008**, *20*, 2719–2726.
(4) Shin, J. H.; Henderson, W. A.; Passerini, S. *Electrochem. Commun.* **2003**, *5*, 1016–1020.
(5) Garcia, B.; Lavallee, S.; Perron, G.; Michot, C.; Armand, M. *Electrochim. Acta* **2004**, *49*, 4583–4588.
(6) Galinski, M.; Lewandowski, A.; Stepniak, I. *Electrochim. Acta* **2006**, *51*, 5567–5580.
(7) De LongH. C. TruloveP. C. SuttoT. E. Ionic Liq. Green Solvents; ACS Symposium Series; American Chemical Society: Washington, DC, 2003, Vol *856*, pp 478−494.
(8) Ding, J.; Zhou, D.; Spinks, G.; Wallace, G.; Forsyth, S.; Forsyth, M.; MacFarlane, D. Use of Ionic Liquids as Electrolytes in Electromechanical Actuator Systems Based on Inherently Conducting Polymers. *Chem. Mater.* **2003**, *1*, 2392–2398.
(9) Cho, M. S.; Seo, H. J.; Nam, J. D.; Choi, H. R.; Koo, J. C.; Song, K. G.; Lee, Y. *Sens. Actuators, B* **2006**, *119*, 621–624.
(10) Liu, Y.; Shi, L. H.; Wang, M. J.; Li, Z. Y.; Liu, H. T.; Li, J. H. *Green Chem.* **2005**, *7*, 655–658.
(11) Hough, W. L.; Rogers, R. D. *Bull. Chem. Soc. Jpn.* **2007**, *80*, 2262–2269.
(12) Marsh, K. N.; Deev, A.; Wu, A. C. T.; Tran, E.; Klamt, A. *Korean J. Chem. Eng.* **2002**, *19*, 357–362.
(13) Schneider, S.; Hawkins, T.; Rosander, M.; Vaghjiani, G.; Chambreau, S.; Drake, G. *Energy Fuels* **2008**, *22*, 2871–2872.
(14) Wang, L.; Huang, Y.; Jia, D. *Electrochim. Acta* **2006**, *51*, 4950–4955.

(15) Bhargava, B. L.; Balasubramanian, S. *J. Chem. Phys.* **2005**, *123*, 144505.
(16) Shah, J. K.; Maginn, E. J. *J. Phys. Chem. B* **2005**, *109*, 10395–10405. Morrow, T. I.; Maginn, E. J. *J. Phys. Chem. B* **2002**, *106*, 12807–12813. Shah, J. K.; Brennecke, J. F.; Maginn, E. J. *Green Chem.* **2002**, *4*, 112–118. Cadena, C.; Anthony, J. L.; Shah, J. K.; Morrow, T. I.; Brennecke, J. F.; Maginn, E. J. *J. Am. Chem. Soc.* **2004**, *126*, 5300–5308.
(17) Del Popolo, M. G.; Lynden-Bell, R. M.; Kohanoff, J. *J. Phys. Chem. B* **2005**, *109*, 5895–5902. Lynden-Bell, R. M.; Kohanoff, J.; Del Popolo, M. G. *Faraday Discuss.* **2005**, *129*, 57–67. Del Popolo, M. G.; Voth, G. A. *J. Phys. Chem. B* **2004**, *108*, 1744–1752. Yan, T. Y.; Burnham, C. J.; Del Popolo, M. G.; Voth, G. A. *J. Phys. Chem. B* **2004**, *108*, 11877–11881.
(18) Kunsagi-Mate, S.; Lemli, B.; Nagy, G.; Kollar, L. *J. Phys. Chem. B* **2004**, *108*, 9246–9250.
(19) Antony, J. H.; Mertens, D.; Breitenstein, T.; Dolle, A.; Wasserscheid, P.; Carper, W. R. *Pure Appl. Chem.* **2004**, *76*, 255–261.
(20) de Andrade, J.; Boes, E. S.; Stassen, H. *J. Phys. Chem. B* **2002**, *106*, 13344–13351. de Andrade, J.; Boes, E. S.; Stassen, H. *Ionic Liquids III A: Fundamentals, Progress, Challenges, and Opportunities, Properties and Structure*; ACS Symposium Series 901; American Chemical Society: Washington, DC, 2005, pp 118−133.
(21) Jensen, M. P.; Neuefeind, J.; Beitz, J. V.; Skanthakumar, S.; Soderholm, L. *J. Am. Chem. Soc.* **2003**, *125*, 15466–15473.
(22) Canongia Lopes, J. N. A.; Deschamps, J.; Padua, A. A. H. *J. Phys. Chem. B* **2004**, *108*, 2038–2047. Canongia Lopes, J. N. A.; Deschamps, J.; Padua, A. A. H. *Ionic Liquids III A: Fundamentals, Progress, Challenges, and Opportunities, Properties and Structure*; ACS Symposium Series 901; American Chemical Society: Washington, DC, 2005, pp 134−149. Deschamps, J.; Padua, A. A. H. *Ionic Liquids III A: Fundamentals, Progress, Challenges, and Opportunities, Properties and Structure*; ACS Symposium Series 901; American Chemical Society: Washington, DC, 2005, pp 150−158. Canongia Lopes, J. N. A.; Padua, A. A. H. *J. Phys. Chem. B* **2006**, *110*, 7485–7489. Deetlefs, M.; Hardacre, C.; Nieuwenhuyzen, M.; Padua, A. A. H.; Sheppard, O.; Soper, A. K. *J. Phys. Chem. B* **2006**, *110*, 12055–12061. Canongia Lopes, J. N. A.; Costa Gomes, M. F.; Padua, A. A. H. *J. Phys. Chem. B* **2006**, *110*, 16816–16818.
(23) Wu, X. P.; Liu, Z. P.; Huang, S. P.; Wang, W. C. *Phys. Chem. Chem. Phys.* **2005**, *7*, 2771–2779.
(24) Hunt, P. A. *Mol. Simul.* **2006**, *32*, 1–10.
(25) Micaelo, N. M.; Baptista, A. M.; Soares, C. M. *J. Phys. Chem. B* **2006**, *110*, 14444–14451.
(26) Rey-Castro, C.; Vega, L. F. *J. Phys. Chem. B* **2006**, *110*, 14426–14435.
(27) Siqueira, L. J. A.; Ribeiro, M. C. C. *J. Phys. Chem. B* **2007**, *11*, 11776–11785.
(28) Bhargava, B. L.; Balasubramanian, S. *J. Chem. Phys.* **2007**, *127*, 114510.
(29) Koddermann, T.; Paschek, D.; Ludwig, R. *ChemPhysChem* **2007**, *8*, 2464–2470.
(30) Bhargava, B. L.; Balasubramanian, S.; Klein, M. L. *Chem. Commun.* **2008**, 3339–3351.
(31) Picálek, J.; Kolafa, J. *J. Mol. Liq.* **2007**, *134*, 29–33.
(32) Borodin, O.; Smith, G. D.; Kim, H. *J. Phys. Chem. B* **2009**, *113*, 4771–4774.
(33) Smith, G. D.; Borodin, O.; Li, L.; Kim, H.; Liu, Q.; Bara, J. E.; Gin, D. L.; Nobel, R. *Phys. Chem. Chem. Phys.* **2008**, *10*, 6301–6312.
(34) Cadena, C.; Zhao, Q.; Snurr, R. Q.; Maginn, E. J. *J. Phys. Chem. B* **2006**, *110*, 2821–2832.
(35) Canongia Lopes, J. N. A.; Padua, A. A. H. *J. Phys. Chem. B* **2004**, *108*, 16893–16898.
(36) Borodin, O.; Smith, G. D. *J. Phys. Chem. B* **2006**, *110*, 11481–11490.
(37) Borodin, O.; Smith, G. D.; Henderson, W. *J. Phys. Chem. B* **2006**, *110*, 16879–16886.
(38) Cadena, C.; Maginn, E. J. *J. Phys. Chem. B* **2006**, *110*, 18026–18039.
(39) Jiang, W.; Yan, T. Y.; Wang, Y. T.; Voth, G. A. *J. Phys. Chem. B* **2008**, *112*, 3121–3131.
(40) Zhou, G. H.; Liu, X. M.; Zhang, S. J.; Yu, G. G.; He, H. Y. *J. Phys. Chem. B* **2007**, *111*, 7078–7084.
(41) Adebahr, J.; Grozema, F. C.; deLeeuw, S. W.; MacFarlane, D. R.; Forsyth, M. *Solid State Ionics* **2006**, *177*, 2845–2850.
(42) Schurhammer, R.; Wipff, G. *J. Phys. Chem. B* **2007**, *111*, 4659–4668.
(43) Siqueira, L. J. A.; Ribeiro, M. C. C. *J. Phys. Chem. B* **2007**, *111*, 11776–11785.
(44) Tsuzuki, S.; Shinoba, W.; Saito, H.; Mikami, M.; Tokuda, H.; Watanabe, M. *J. Phys. Chem. B.* **2009**, *113*, 10641–10649.
(45) Cadena, C.; Anthony, J. L.; Shah, J. K.; Morrow, T. I.; Brennecke, J. F.; Maginn, E. J. *J. Am. Chem. Soc.* **2004**, *126*, 5300–5308.
(46) Zhao, W.; Leroy, F.; Heggen, B.; Zahn, S.; Kirchner, B.; Balasubramanian, S.; Muller-Plathe, F. *J. Am. Chem. Soc.* **2009**, *131*, 15825–15833.
(47) Borodin, O. *J. Phys. Chem. B* **2009**, *113*, 11463–11478.
(48) Iuchi, S.; Izvekov, S.; Voth, G. A. *; J. Chem. Phys.* **2007**, *126*, 124505.
(49) Izvekov, S.; Parrinello, M.; Burnham, C. J.; Voth, G. A. *J. Chem. Phys.* **2004**, *120*, 10896.
(50) Aguado, A.; Wilson, M.; Maddane, P. A. *J. Chem. Phys.* **2001**, *115*, 8603.
(51) Morgan, B.; Madden, P. A. *J. Chem. Phys.* **2004**, *120*, 1402.
(52) Yan, T.; Burnham, C. J.; Del Popolo, M. G.; Voth, G. A. *J. Phys. Chem. B.* **2004**, *108*, 11877.
(53) Yan, T.; Li, S.; Jiang, W.; Gao, X.; Xiang, B.; Voth, G. A. *J. Phys. Chem. B* **2006**, *110*, 1800.
(54) Borodin, O. In Molecular Dynamics Simulations of Ionic Liquids: Influence of Polarization on IL Structure and Ion Transport. *Materials Research Society Spring Meeting, San Francisco, 2008*; Baker, G. A., H. Yang, J. S. W., Eds.; MRS: San Francisco, 2008; pp Q06−04.
(55) Hansen, J.-P.; McDonald, I. R. *Theory of Simple Liquids*; Elsevier Academic Press: The Netherlands, 2007; Chapter 10.
(56) Shiflett, M. B.; Yokozeki, A. *J. Chem. Eng. Data* **2007**, *52*, 1302–1306.
(57) Zhou, Z. B.; Matsumoto, H.; Tatsumi, K. *ChemPhysChem* **2005**, *6*, 1324–1332.
(58) Matsumoto, H.; Sakaebe, H.; Tatsumi, K.; Kikuta, M.; Ishiko, E.; Kono, M. *J. Power Sources* **2006**, *160*, 1308–1313.
(59) Yoshida, Y.; Baba, O.; Saito, G. *J. Phys. Chem. B* **2007**, *111*, 4742–4749.
(60) Bazito, F. F. C.; Kawano, Y.; Torresi, R. M. *Electrochim. Acta* **2007**, *52*, 6427–6437.
(61) Tokuda, H.; Ishii, K.; Susan, M. A. B. H.; Tsuzuki, S.; Hayamizu, K.; Watanabe, M. *J. Phys. Chem. B* **2006**, *110*, 2833–2839.
(62) Wang, Y. D.; Zaghib, K.; Guerfi, A.; Bazito, F. F. C.; Torresi, R. M.; Dahn, J. R. *Electrochim. Acta* **2007**, *52*, 6346–6352.
(63) Borodin, O.; Smith, G. D. *J. Phys. Chem. B* **2006**, *110*, 6279–6292.
(64) Dang, L. X. *J. Chem. Phys.* **1992**, *97*, 2659.
(65) Smith, D. E.; Dang, L. X. *J. Chem. Phys.* **1994**, *100*, 3757.
(66) Wang, Y.; Izvekov, S.; Yan, T.; Voth, G. A. *J. Phys. Chem. B.* **2006**, *110*, 3564. Izvekov, S.; Voth, G. A. *J. Chem. Phys.* **2005**, *123*, 134105.
(67) Press, W. H.; Flannery, B. P.; Teukolsky S. A.; Vetterling W. T. *Numerical Recipes: The Art of Scientific Computing*; Cambridge University Press: New York, 1986.
(68) http://www.eng.utah.edu/∼gdsmith/lucretius.html.
(69) Palmer, B. J. *J. Comput. Phys.* **1993**, *104*, 470.
(70) Martyna, G. J.; Tuckerman, M. E.; Tobias, D. J.; Klein, M. L. *Mol. Phys.* **1996**, *87*, 1117.
(71) Martyna, G. J.; Tobias, D. J.; Klein, M. L. *J. Chem. Phys.* **1994**, *101*, 4177.
(72) Borodin, O. *J. Phys. Chem. B* **2009**, *113*, 12353–12357.
(73) McQuarrie, D. A. *Statistical Mechanics*, Harper & Row: New York, 1976.

JP911670F